Supplementary Information (SI) for Chemical Science.
This journal is © The Royal Society of Chemistry 2026

Electronic Supplementary Information

Stepwise B≡N bond cleavage by isocyanides: access to the 3-azaborole structural motif

Libo Xiang,[a] Kwan Ka Ho,[b] Yi Jing,[c] Junyi Wang,[d] Alexander Matler,[a] Xuenian Chen,[c] Zhenyang Lin*,[b] Qing Ye*,[a]

[a]Institute for Inorganic Chemistry and Institute for Sustainable Chemistry & Catalysis with Boron, Julius-Maximilians-Universität Würzburg, 97074 Würzburg Germany

[b]Department of Chemistry, The Hong Kong University of Science and Technology, Clear Water Bay, Kowloon, Hong Kong

[c] College of Chemistry, Zhengzhou University, 450001, Zhengzhou, Henan (P. R. China)

[d] Department of Chemistry, Southern University of Science and Technology, 518055, Shenzhen, Guangdong (P. R. China)

Table of Contents

Experimental Procedures

General considerations. All manipulations were conducted either under an atmosphere of dry argon or in *vacuo* using standard Schlenk line or glovebox techniques. Solvents were purified by distillation from Na/K under dry argon. C_6D_6 and toluene-d_8 were degassed by three freeze-pump-thaw cycles and stored over molecular sieves. Borirane **1**, was prepared according to published procedures.[1] NMR spectra were acquired on a Bruker Avance 400 (^{1}H: 400.1 MHz, ^{11}B: 128.4 MHz, ^{13}C: 100.6 MHz) NMR spectrometer at 298 K without mentioned. ^{1}H, ^{13}C{^{1}H} and ^{1}H{^{11}B} spectra were referenced to external TMS. ^{11}B and ^{11}B{^{1}H} NMR spectra were referenced to external $BF_3{\cdot}OEt_2$. High-resolution mass spectrometry (HRMS) was performed with a Thermo Fisher Scientific Q-Exactive MS System. Elemental analysis (C, H, N) was performed on a vario micro cube CHNS analyzer. Cyclic voltammetry experiments were performed using a Gamry Instruments Reference 600 potentiostat. UV-vis absorption spectra were recorded on a Thermo Scientific Evolution 201 UV-Visible Spectrophotometer.

Synthesis of 2

Mes*NC (27 mg, 1.0 eq, 0.10 mmol) was added to iminoborane **1** (32 mg, 1.0 eq, 0.10 mmol) in 2 mL pentane at room temperature. After mixing thoroughly, the reaction system was stored overnight under −30 °C for 12 h. Analytically pure product was isolated as orange block crystals **2**.

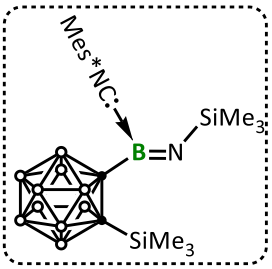

2, 49 mg, 84%, **^{1}H NMR** (C_6D_6): δ = 7.39 (*s*, 2H, C_6H_2), 3.58 to 1.78 (*m*, 10H, B*H*), 1.51 (*s*, 18H, *o*-C(C*H*$_3$)$_3$), 1.19 (*s*, 9H, *p*-C(C*H*$_3$)$_3$), 0.07 (*s*, 9H, Si*Me*$_3$), 0.06 (*s*, 9H, Si*Me*$_3$); **^{1}H{^{11}B} NMR** (C_6D_6): δ = 7.39 (*s*, 2H, C_6H_2), 3.17 (*s*, 1H, B*H*), 3.10 (*s*, 1H, B*H*), 2.93 (*s*, 2H, B*H*), 2.64 (*s*, 2H, B*H*), 2.50 (*s*, 2H, B*H*), 2.30 (*s*, 2H, B*H*), 1.52 (*s*, 18H, *o*-C(C*H*$_3$)$_3$), 1.19 (*s*, 9H, *p*-C(C*H*$_3$)$_3$), 0.06 (*s*, 18H, Si*Me*$_3$); **^{11}B NMR** (C_6D_6): δ = 13.4 (*s*, Cb*B*NSiMe$_3$), 3.9 (*d*, *J* = 142.3 Hz, *B*$_{Cb}$), 1.5 (*d*, *J* = 155.0 Hz, *B*$_{Cb}$), −5.6 (*d*, *J* = 152.2 Hz, *B*$_{Cb}$), −8.0 to −11.1 (*m*, *B*$_{Cb}$); **^{11}B{^{1}H} NMR** (C_6D_6): δ = 13.8 (*s*, Cb*B*NSiMe$_3$), 4.0 (*s*, *B*$_{Cb}$), 1.6 (*s*, *B*$_{Cb}$), −5.5 (*s*, *B*$_{Cb}$), −8.6 (*s*, *B*$_{Cb}$),

–9.7 (*s*, *B*Cb), –10.5 (*s*, *B*Cb); **^{13}C{^{1}H} NMR** (C_6D_6): δ = 176.1 (*C* of Ph), 151.5 (*C* of Ph), 147.6 (*C* of Ph), 122.1 (*C* of Ph), 72.8 (*C* of Cb), 35.8 ($C(CH_3)_3$), 35.3 ($C(CH_3)_3$), 31.2 ($C(CH_3)_3$), 29.5 ($C(CH_3)_3$), 1.3 (Si*Me*$_3$), –0.5 (Si*Me*$_3$); **Elemental analysis**: calcd. for $C_{27}H_{57}B_{11}N_2Si_2$: C, 55.45; H, 9.82; N, 4.79; found: C, 54.29; H, 9.72; N, 4.89.

Synthesis of 3

RNC (3.0 eq, 0.3 mmol) in toluene was added to a toluene solution of **1** (32 mg, 1.0 eq, 0.1 mmol) at −30 °C and the solution immediately turned to yellow. After thoroughly mixing, the reaction was stored at −30 °C for 12 h, resulting in the formation of yellow crystals. Then, the mother liquid was removed and the solid was dried under vacuum to yield yellow crystals of **3** (74 mg, 0.9 mmol, 89%).

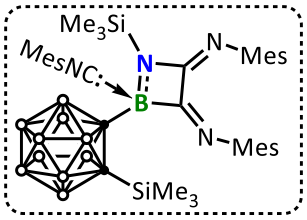

3a (R = Mes, 64 mg, 89%) **^{1}H NMR** (400 MHz, C_6D_6): δ [ppm] = 6.58 to 6.28 (*m*, 4H, C_6H_3), 6.27 (*s*, 2H, C_6H_3), 3.97 to 2.38 (*m*, 10H, B*H*), 2.16 (*s*, 3H, CH_3), 2.13 (*s*, 3H, CH_3), 2.11 (*s*, 9H, CH_3), 2.05 (*s*, 9H, CH_3), 1. 80 (*s*, 3H, CH_3), 0.54 (*s*, 9H, Si(CH_3)$_3$), 0.31 (*s*, 9H, Si(CH_3)$_3$). **^{1}H{^{11}B} NMR** (400 MHz, C_6D_6): δ [ppm] = 6.58 to 6.28 (*m*, 4H, C_6H_3), 6.26 (*s*, 2H, C_6H_3), 3.97 to 2.38 (*m*, 10H, B*H*), 3.40 (*br*, s, 1H, B*H*), 3.30 (*br*, s, 1H, B*H*), 3.20 (*br*, 2H, B*H*), 3.01 (*br*, 4H, B*H*), 2.62 (*br*, 2H, B*H*), 2.16 (*s*, 3H, CH_3), 2.13 (*s*, 3H, CH_3), 2.12 (*s*, 9H, CH_3), 2.04 (*s*, 9H, CH_3), 1.80 (*s*, 3H, CH_3), 0.54 (*s*, 9H, Si(CH_3)$_3$), 0.31 (*s*, 9H, Si(CH_3)$_3$). **^{11}B NMR** (128 MHz, C_6D_6): δ [ppm] = 1.67 (*br*, *B*Cb), –5.91 (*br*, *B*Cb), –8.48 (*br*, *B*Cb). **^{11}B{^{1}H} NMR** (128 MHz, C_6D_6): δ [ppm] = 2.30 (*s*, *B*Cb), 0.80 (*s*, *B*Cb), –5.19 (*br*, *B*Cb), –8.36 (*br*, *B*Cb). **^{13}C NMR{^{1}H}** (101 MHz, C_6D_6): δ [ppm] = 137.5, 128.9, 128.2, 127.8, 127.6 (*C* of C_6H_2), 125.3 (*C*H of C_6H_2), 31.6, 22.7, 21.1, 20.6, 19.4, 18.3, 14.0, 1.7, 1.3 (Si*Me*$_3$); **Elemental analysis**: calcd. For $C_{38}H_{61}B_{11}N_4Si_2$: C, 60.94; H, 8.21; N,7.48; found: C, 60.80; H, 8.30; N, 7.33.

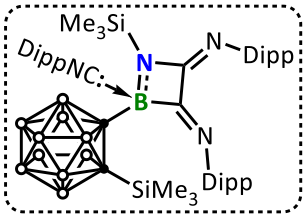

3b (R = 56mg, 64%) **^{1}H NMR** (C_6D_6): δ = 7.07 to 6.80 (*m*, 9H, C*H* of Dipp), 3.38 (s*ept*, *J* = 6.8 Hz, 2H, $CH(CH_3)_2$), 3.76 to 2.14 (*m*, 10H, B*H*), 3.09 (*br*, 1H, C(*H*)(CH_3)$_2$), 2.80 (*br,* 1H, C(*H*)(CH_3)$_2$), 1.26 (*br*, 12H, C(H)(CH_3)$_2$), 1.13 (*br*, 6H, C(H)(CH_3)$_2$), 1.05 (*d*, *J* = 6.9 Hz, 12H, CH(CH_3)$_2$), 0.93 (*br*, 6H, C(H)(CH_3)$_2$), 0.45 (*s*, 9H, Si*Me*$_3$), 0.07 (*s*, 9H, Si*Me*$_3$); **^{1}H{^{11}B} NMR** (C_6D_6): δ = 7.06 to 6.81 (*m*, 9H, C*H* of Dipp), 3.38 (s*ept*, *J* = 6.8 Hz, 2H, $CH(CH_3)_2$), 3.10 (*br*, 6H, 4H of C(*H*)(CH_3)$_2$ and 2H of B*H*), 2.75 (*br*, 2H, B*H*), 2.63 (*br*, 3H, B*H*), 2.39 (*br*, 3H, B*H*), 2.19 (*br*, 2H, B*H*), 1.25 (*br*, 12H, C(H)(CH_3)$_2$), 1.13 (*m*, 6H, C(H)(CH_3)$_2$), 1.06 (*d*, *J* = 6.9 Hz, 12H, CH(CH_3)$_2$), 0.91 (*br*, 6H, C(H)(CH_3)$_2$), 0.45 (*s*, 9H, Si*Me*$_3$), 0.07 (*s*, 9H, Si*Me*$_3$); **^{11}B NMR** (C_6D_6): δ = –1.80 (*d*, *J* = 141.16 Hz, *B*Cb), –7.96 (*d*, *J* = 156.19 Hz, *B*Cb), –10.30 (*br*, *B*Cb), –14.82 (*d*, *J* = 106.89 Hz, *B*Cb); **^{11}B{^{1}H} NMR** (C_6D_6): δ = –1.86 (s, *B*Cb), –8.10 (*s*, *B*Cb), –9.47 (*s*, *B*Cb), –11.56 (*s*, *B*Cb), –14.76 (*s*, *B*Cb); **^{13}C NMR{^{1}H}** (C_6D_6): δ = 131.3, 128.9, 128.2, 127.6, 127.3 (*C* of C_6H_3), 123.4, 122.2, 31.6, 29.7, 28.6, 28.5 (*C*H(CH_3)$_2$), 23.5, 22.4, 14.0, (CH(*C*H_3)$_2$), 1.4, 0.0 (Si*Me*$_3$); **HRMS (LIFDI)**: calcd. For $C_{47}H_{79}N_4B_{11}Si_2$, 876.6867; found 876.6909.

Synthesis of 4a

Calcium (4 mg, 1.0 eq, 0.1 mmol) was cut by a scissor into small pieces and added to a THF solution of **3a** (74 mg, 1.0 eq, 0.1 mmol). The reaction mixture was stirred at room temperature for 5 days, during which time the solution slowly turned purple. Then, filtered out the excess calcium and removed the solvent under vacuum. The residue

was washed with toluene and THF, followed by extraction with MeCN, and the solution was stored at −30 °C overnight for crystallization. Purple crystals of **4a** (41 mg, 0.04 mmol, 42%) appeared.

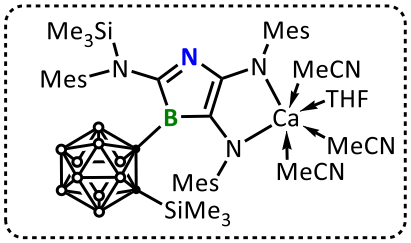

^{1}H NMR (400 MHz, CD_3CN): δ [ppm] = 6.85 (*s*, 1H, C_6H_2), 6.81 (*s*, 2H, C_6H_2), 6.76 (*s*, 1H, C_6H_2), 6.70 (*s*, 1H, C_6H_2), 6.68 (*s*, 1H, C_6H_2), 3.66 to 3.63 (*m*, 4H, CH_2 of THF), 2.65 to 0.51 (*br*, 10H, B*H*), 2.44 (*s*, 3H, CH_3), 2.32 (*s*, 3H, CH_3), 2.24 (*s*, 6H, CH_3), 2.22 (s, 3H, CH_3), 2.20 (*s*, 3H, CH_3), 2.08 (*s*, 3H, CH_3), 1.99 (*s*, 3H, CH_3), 1.96 (s, 9 H, H of MeCN and CH_3), 1.82 to 1.79 (*m*, 4H, CH_2 of THF), −0.01 (*s*, 9H, SiMe_3) −0.25 (*s*, 9H, Si(CH_3)$_3$). **^{1}H{^{11}B} NMR** (400 MHz, CD_3CN): δ [ppm] = 6.84 (*s*, 1H, C_6H_2), 6.80*s*, 2H, C_6H_2), 6.75 (*s*, 1H, C_6H_2), 6.70 (*s*, 1H, C_6H_2), 6.67 (*s*, 1H, C_6H_2), 3.66 to 3.62 (*m*, 4H, CH_2 of THF), 2.44 (*s*, 3H, CH_3), 2.32 (*s*, 3H, CH_3), 2.22 (*s*, 6H, CH_3), 2.24 (*s*, 3H, CH_3), 2.20 (*s*, 3H, CH_3), 2.07 (*s*, 3H, CH_3), 1.99 (*s*, 3H, CH_3), 1.96 (s, 9 H, H of MeCN and CH_3), 1.81 to 1.78 (*m*, 4H, CH_2 of THF), 1.41 (*s*, 2H, B*H*), 1.27 (*s*, 1H, B*H*), 0.81 (*s*, 1H, B*H*), 0.58 (*s*, 1H, B*H*), −0.01 (*s*, 9H, SiMe_3) −0.26 (*s*, 9H, Si(CH_3)$_3$). **^{11}B NMR** (128 MHz, CD_3CN): δ [ppm] = 29.81 (*br*, Cb*B*C_3N), 0.80 to −14.90 (*m*, B_{Cb}), −26.80 (*d*, *J* = 125.36 Hz, B_{Cb}). **^{11}B{^{1}H} NMR** (128 MHz, CD_3CN): δ [ppm] = 29.88 (*br*, Cb*B*C_3N), −0.93 (*s*, B_{Cb}), −9.41 (*s*, B_{Cb}), −11.07 (*s*, B_{Cb}), −12.10 (*s*, B_{Cb}) −26.78 (*s*, B_{Cb}). **^{13}C NMR{^{1}H}** (101 MHz, CD_3CN): δ [ppm] = 140.8, 137.5, 137.4, 135.5, 131.9, 131.7, 129.9, 129.5, 129.2, 128.7, 128.7, 128.4, 126.3, 66.3 (*C* of Cb), 21.7, 21.1, 21.0, 20.8, 20.3, 19.9, 19.7, 19.5, 15.6, 3.4 (SiMe_3), −0.7 (SiMe_3). **Elemental analysis**: calcd. for $C_{48.55}H_{79.37}B_{11}N_{6.73}O_{1.27}Si_2Ca$ • $C_4H_6N_2$: C, 58. 65; H, 7.94; N, 11.82; found: C, 58.25; H, 7.91; N, 10.90. Note: The single-crystal X-ray structure revealed two non-coordinated acetonitrile molecules per formula unit. However, elemental analysis gave a lower nitrogen content than calculated, consistent with partial loss of solvent molecules upon drying and the sensitivity of the sample.

Synthesis of 4b

Mg(An)(THF)$_3$ (42 mg, 1.0 eq, 0.1 mmol) was added to a THF solution of **3** (74 mg, 1.0 eq, 0.1 mmol) and stirred at room temperature and the solution turned to purple in 10 min. The reaction system was stirred overnight at room temperature after the solution was thoroughly mixed. After removal of the solvent under vacuum, the residue was washed with hexane, toluene and THF, followed by extracted with CH_3CN, and stored at −30 °C overnight for crystallization. Purple crystals appeared, small amount of anthracene was removed using cold CH_3CN, yielding compound **4b** (30 mg, 0.03 mmol, 31%).

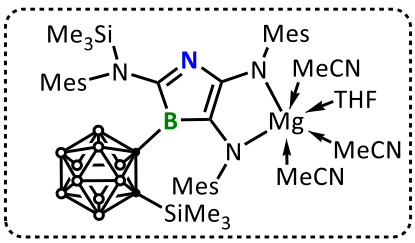

^{1}H NMR (400 MHz, CD_3CN): δ [ppm] = 6.86 (*s*, 1H, C_6H_2), 6.82 (*s*, 1H, C_6H_2), 6.80 (*s*, 1H, C_6H_2), 6.76 (*s*, 1H, C_6H_2), 6.70 (*s*, 1H, C_6H_2), 6.68 (*s*, 1H, C_6H_2), 3.66 to 3.63 (*m*, 4H, CH_2 of THF), 2.61 to 0.80 (*m*, B*H*), 2.49 (*s*, 3H, CH_3), 2.32 (*s*, 3H, CH_3), 2.24 (*s*, 6H, CH_3), 2.23 (*s*, 3H, CH_3), 2.20 (*s*, 3H, CH_3), 2.11 (*s*, 3H, CH_3), 2.00 (*s*, 3H, CH_3), 1.96 (s, 9 H, H of MeCN and CH_3), 1.79 to 1.82 (*m*, 4H, CH_2 of THF), −0.01 (*s*, 9H, Si(CH_3)$_3$), −0.24 (*s*, 9H, Si(CH_3)$_3$). **^{1}H{^{11}B} NMR** (400 MHz, CD_3CN): δ [ppm] = 6.86 (*s*, 1H, C_6H_2), 6.82 (*s*, 1H, C_6H_2), 6.80 (*s*, 1H, C_6H_2), 6.76 (*s*, 1H, C_6H_2), 6.70 (*s*, 1H, C_6H_2), 6.68 (*s*, 1H, C_6H_2), 3.66 to 3.63 (*m*, 4H, CH_2 of THF), 2.49 (*s*, 3H, CH_3), 2.32 (*s*, 3H, CH_3), 2.24 (*s*, 6H, CH_3), 2.23 (*s*, 3H, CH_3), 2.20 (*s*, 3H, CH_3), 2.11 (*s*, 3H, CH_3), 2.00 (*s*, 3H, CH_3), 1.96 (s, 9 H, H of MeCN and CH_3), 1.82 to 1.79 (*m*, 4H, CH_2 of THF), 1.45 (*s*, 2H, B*H*), 1.27 (*s*, 1H, B*H*), 0.79 (*s*, 1H, B*H*), −0.01

(*s*, 9H, Si(CH_3)$_3$), −0.24 (*s*, 9H, Si(CH_3)$_3$). **^{11}B NMR** (128 MHz, THF): δ [ppm] = 26.94 (*s*, Cb*B*C$_3$N), 1.51 (*d*, *J* = 156.19 Hz, *B*$_{Cb}$), −5.61 (*br*, *B*$_{Cb}$), −9.43 (*br*, *B*$_{Cb}$), −21.82 (*br*, *B*$_{Cb}$). **^{11}B{^{1}H} NMR** (128 MHz, THF): δ [ppm] = 26.65 (*s*, Cb*B*C$_3$N), 1. 37 (*s*, *B*$_{Cb}$), −5.11 (*s*, *B*$_{Cb}$), −9.00 (*s*, *B*$_{Cb}$), −21.82 (*s*, *B*$_{Cb}$). **^{13}C{^{1}H} NMR**: ^{13}C NMR spectrum was not obtained due to poor solubility in THF and acetonitrile. **Elemental analysis**: calcd. for $C_{48}H_{78}B_{11}N_7OMgSi_2$: C, 59.52; H, 8.12; N, 10.12; found: C, 59.01; H, 8.15; N, 10.72.

NMR and IR Spectra

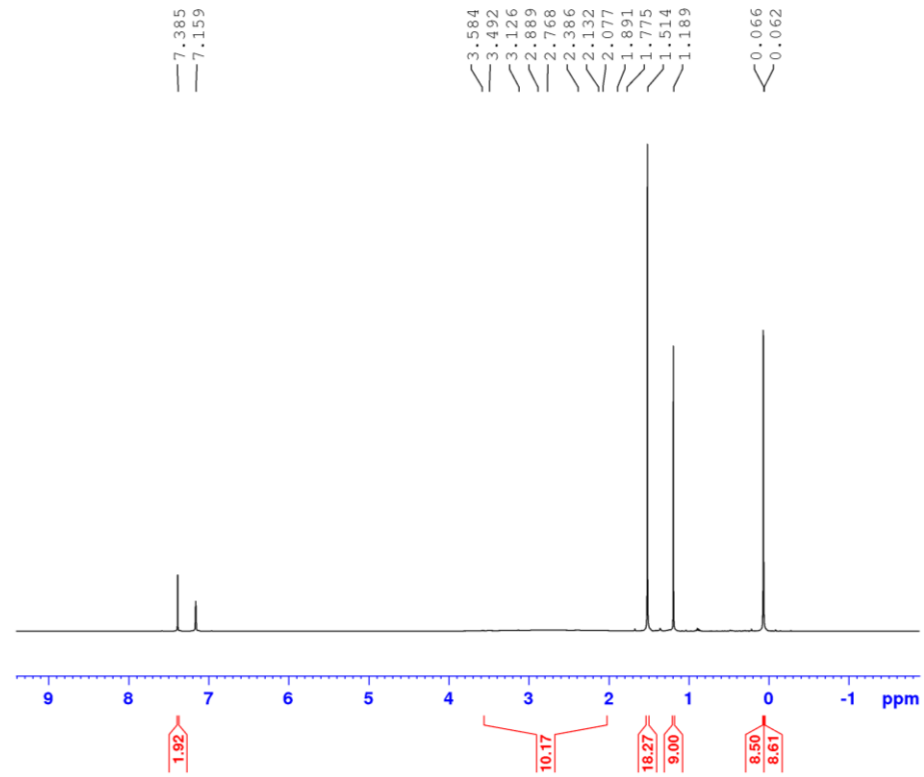

Figure S1. ^{1}H NMR spectrum of **2** in C_6D_6

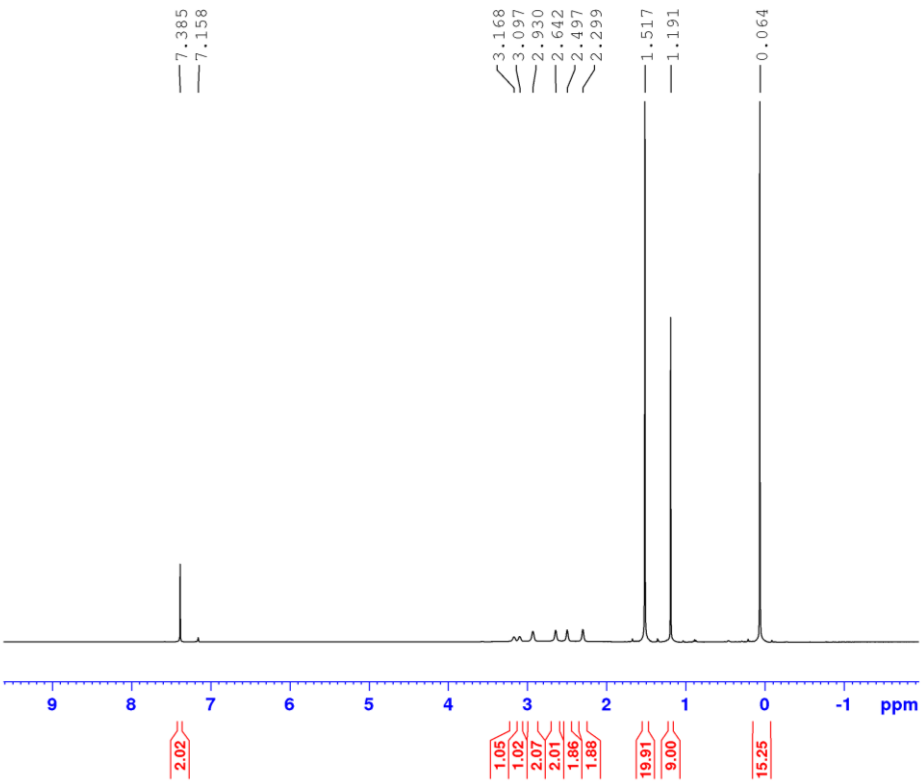

Figure S2. $^{1}H\{^{11}B\}$ NMR spectrum of **2** in C_6D_6

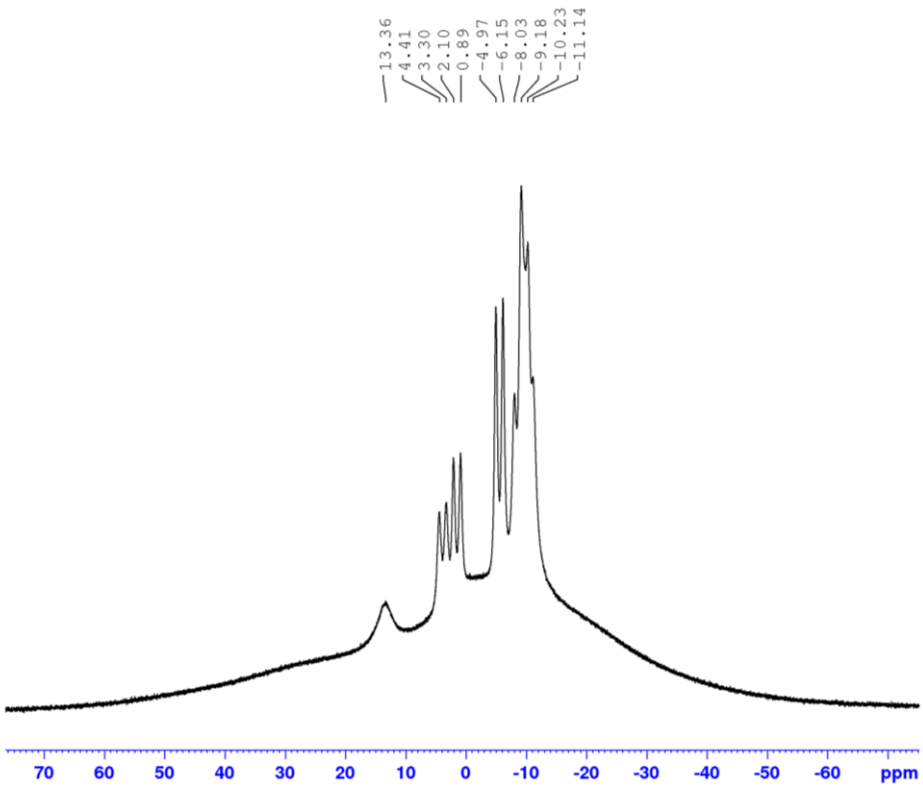

Figure S3. ^{11}B NMR spectrum of **2** in C_6D_6

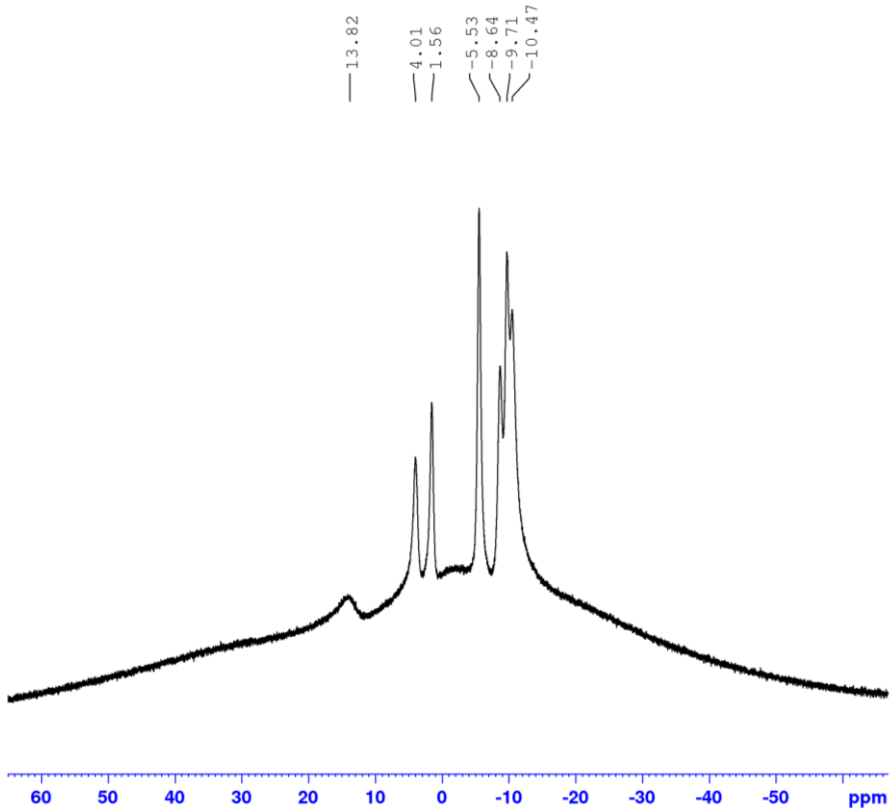

Figure S4. $^{11}B\{^1H\}$ NMR spectrum of **2** in C_6D_6

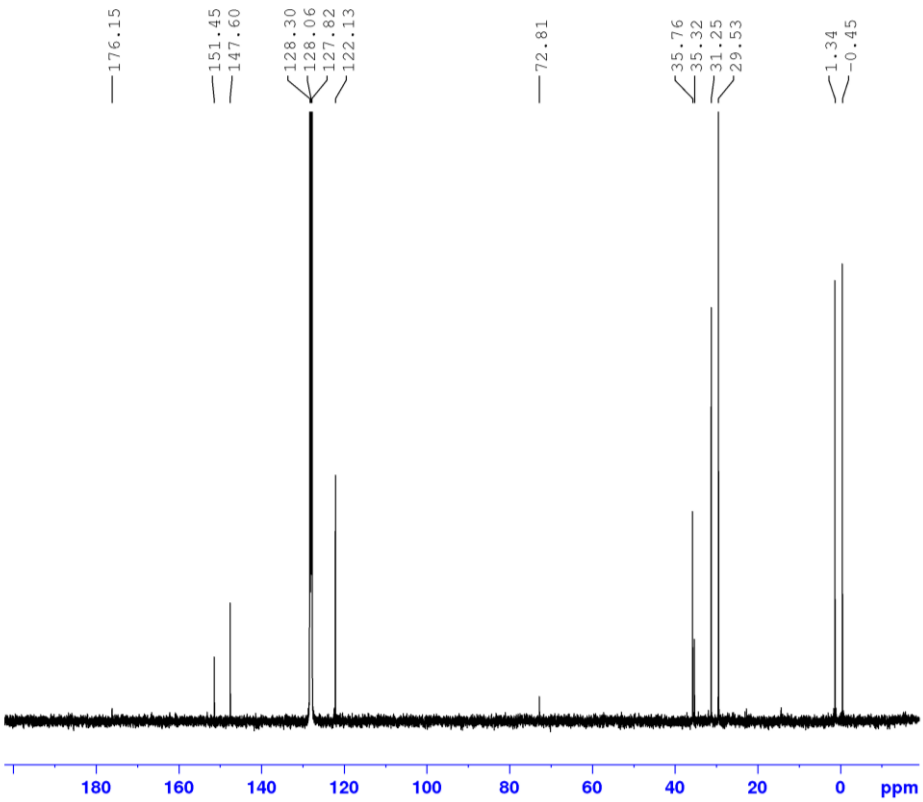

Figure S5. $^{13}C\{^{1}H\}$ NMR spectrum of **2** in C_6D_6

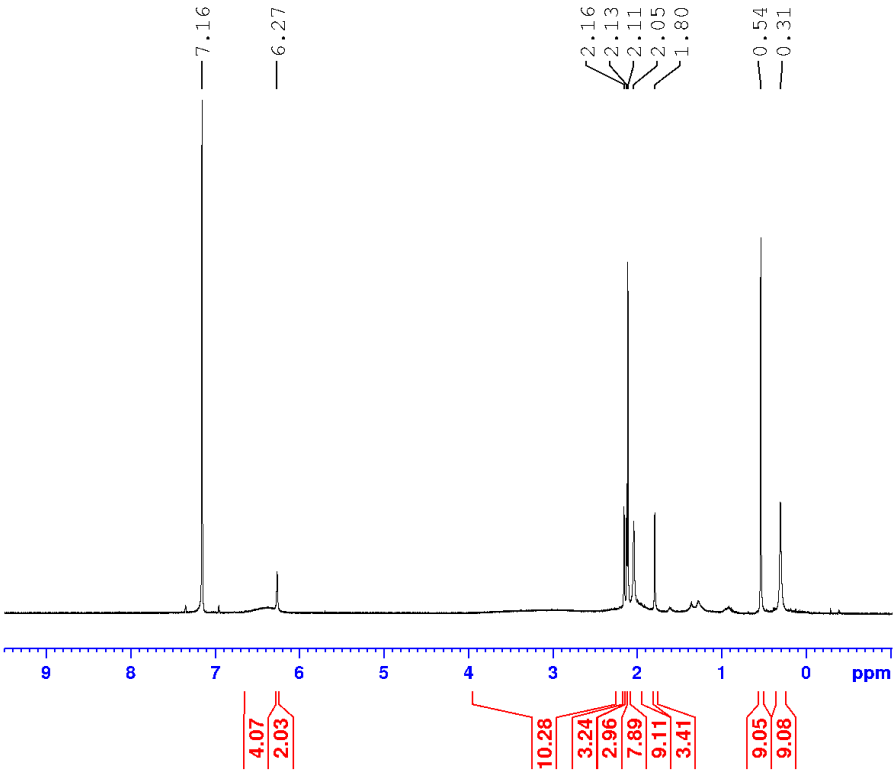

Figure S6. ^{1}H NMR spectrum of **3a** in C_6D_6

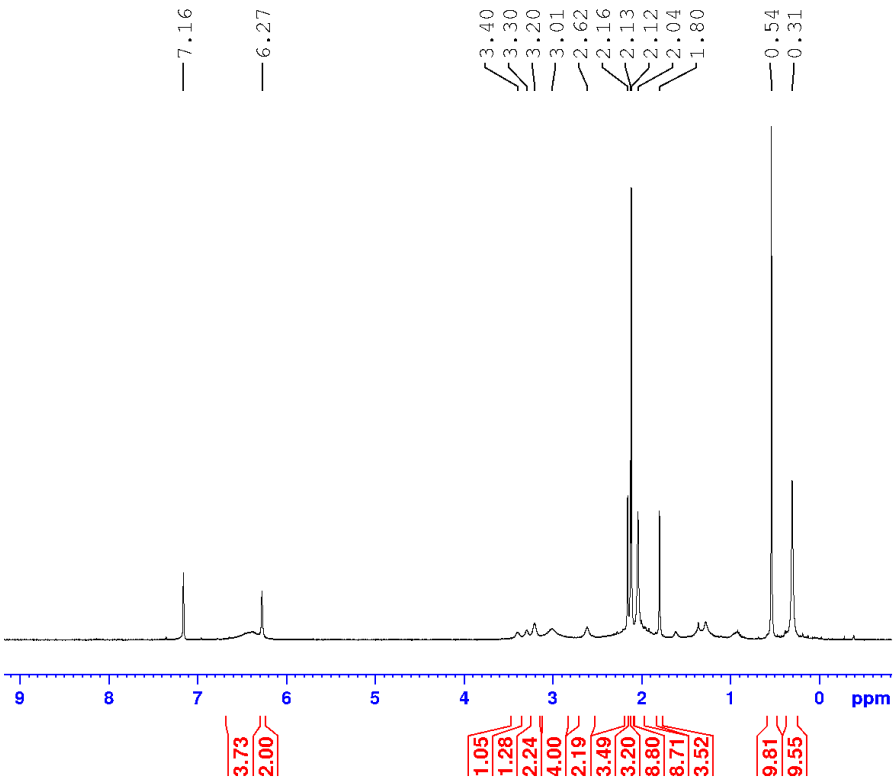

Figure S7. $^{1}H\{^{11}B\}$ NMR spectrum of **3a** in C_6D_6

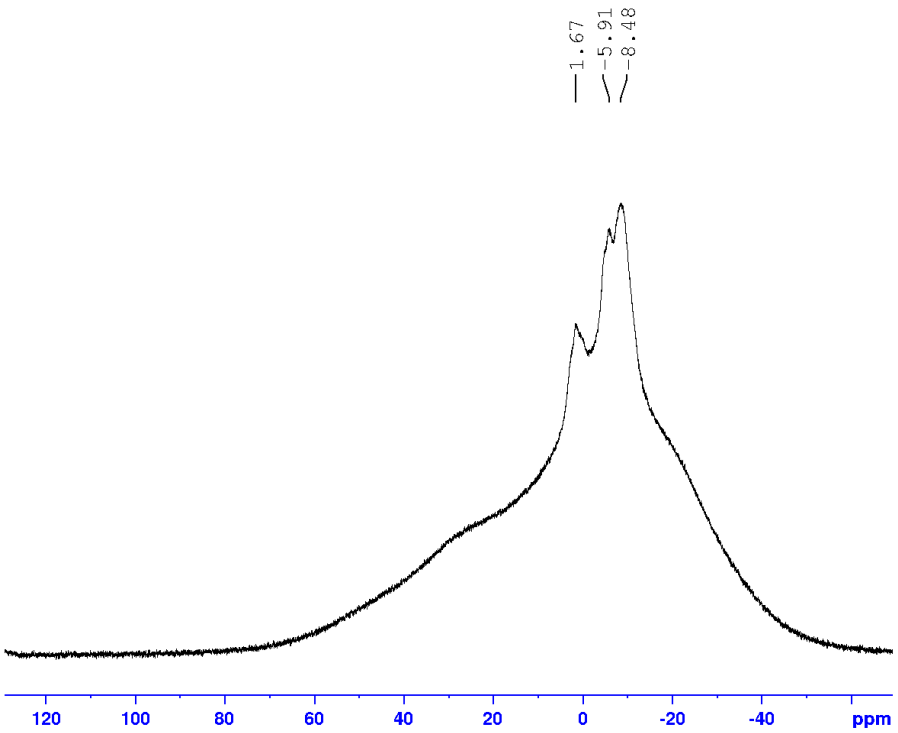

Figure S8. ^{11}B NMR spectrum of **3a** in C_6D_6

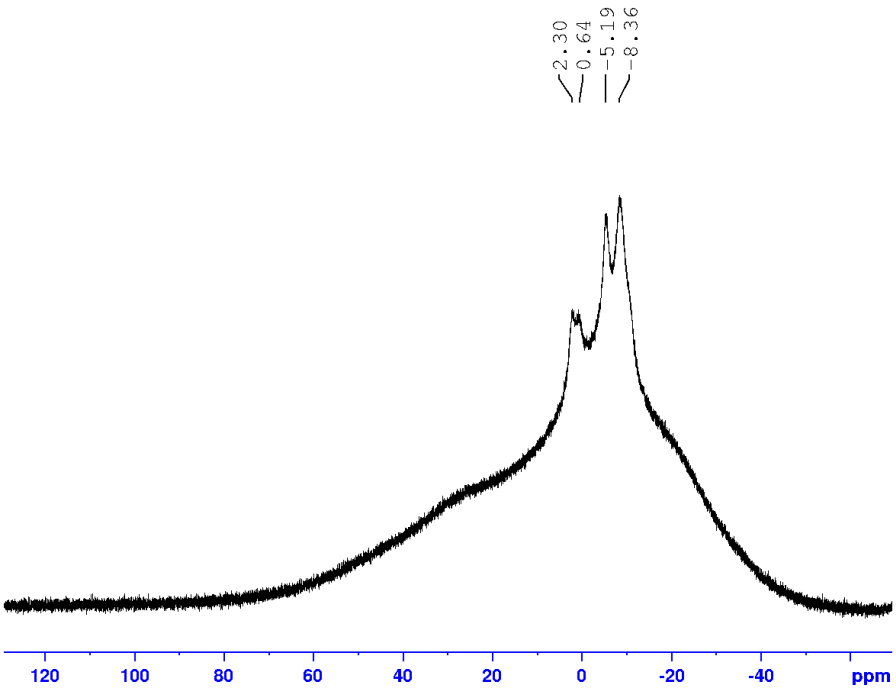

Figure S9. $^{11}B\{^{1}H\}$ NMR spectrum of **3a** in C_6D_6

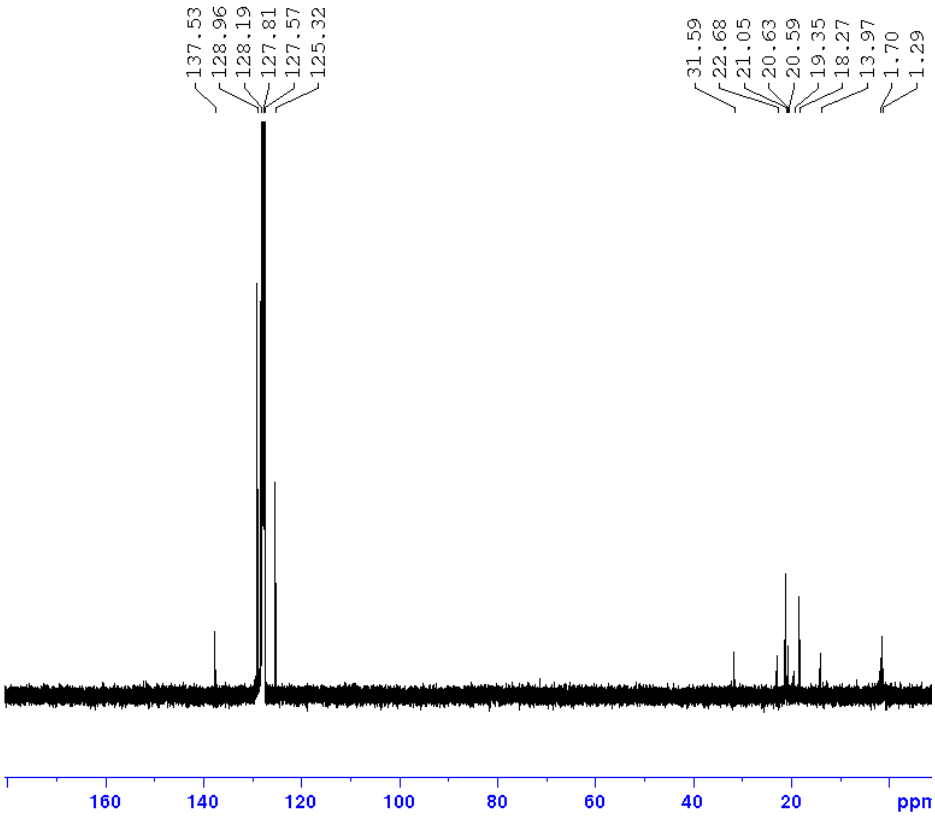

Figure S10. $^{13}C\{^{1}H\}$ NMR spectrum of **3a** in C_6D_6

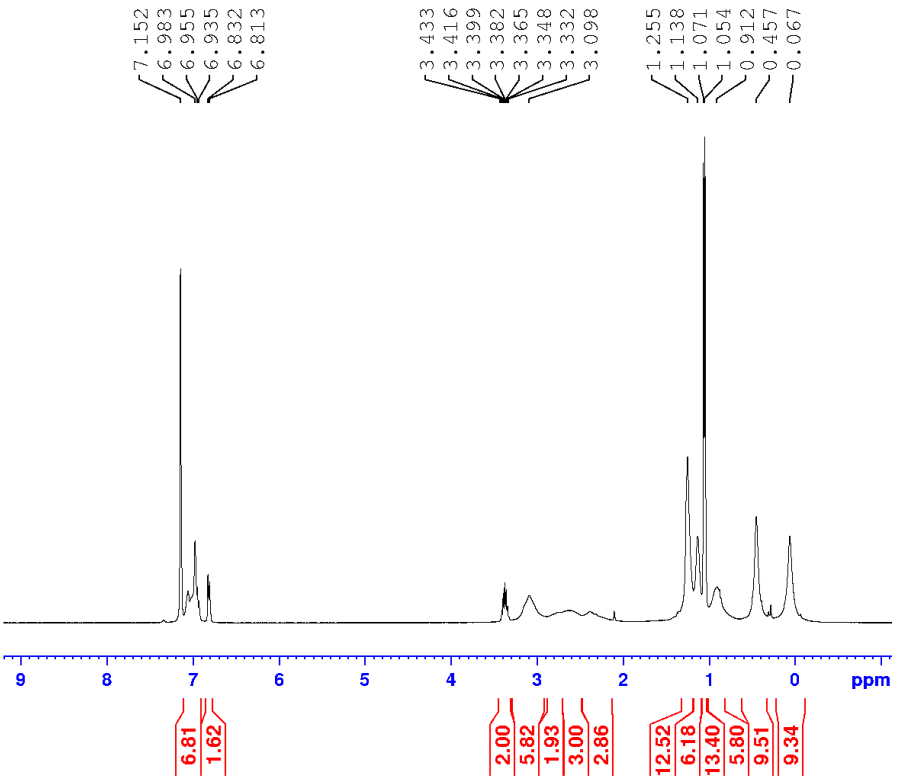

Figure S11. ^{1}H NMR spectrum of **3b** in C_6D_6

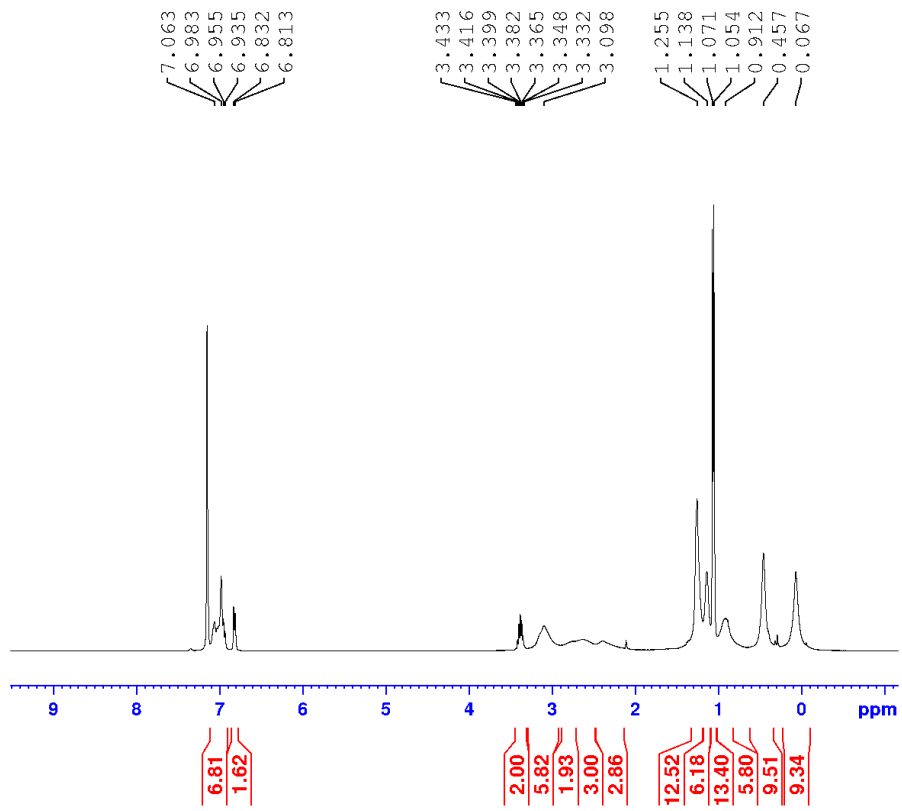

Figure S12. $^{1}H\{^{11}B\}$ NR spectrum of **3b** in C_6D_6

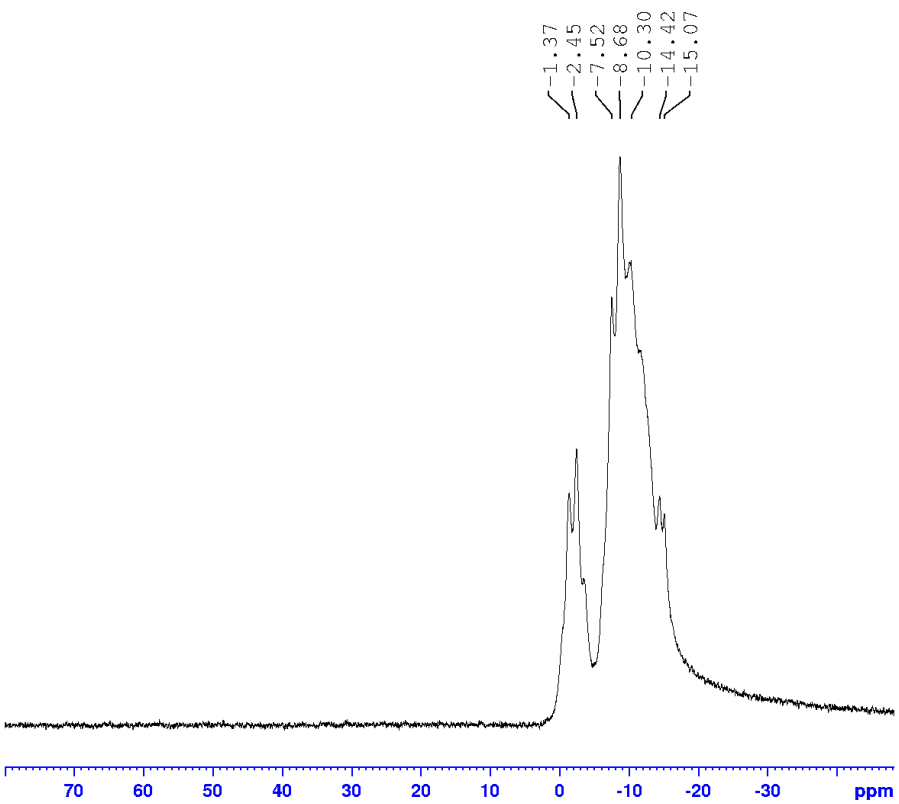

Figure S13. ^{11}B NMR spectrum of **3b** in C_6D_6

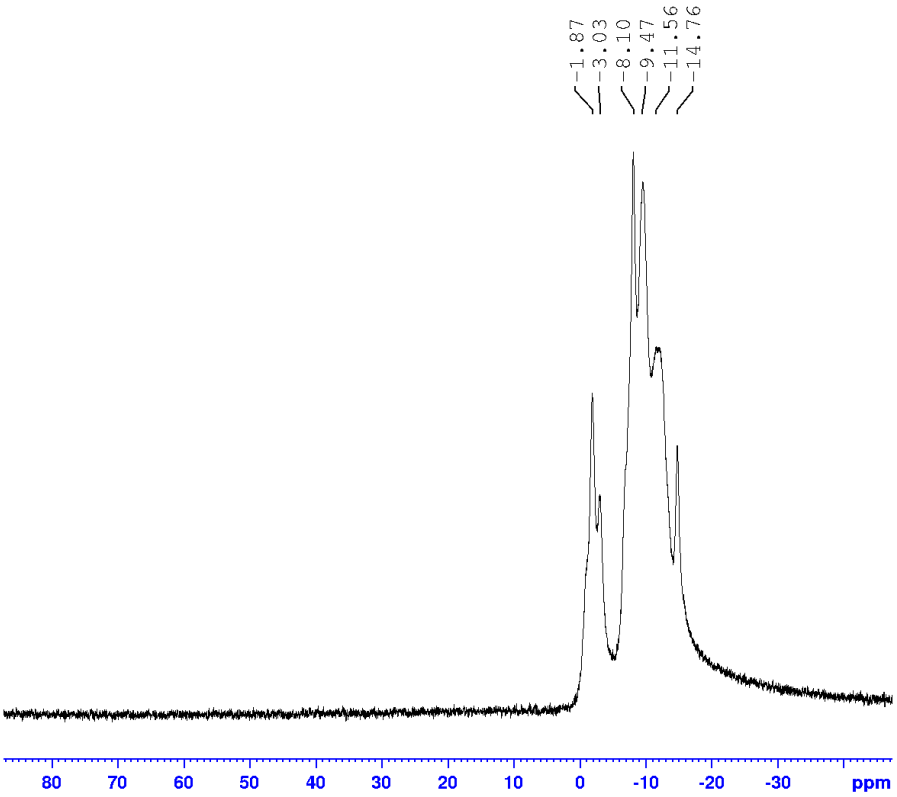

Figure S14. $^{11}B\{^1H\}$ NMR spectrum of **3b** in C_6D_6

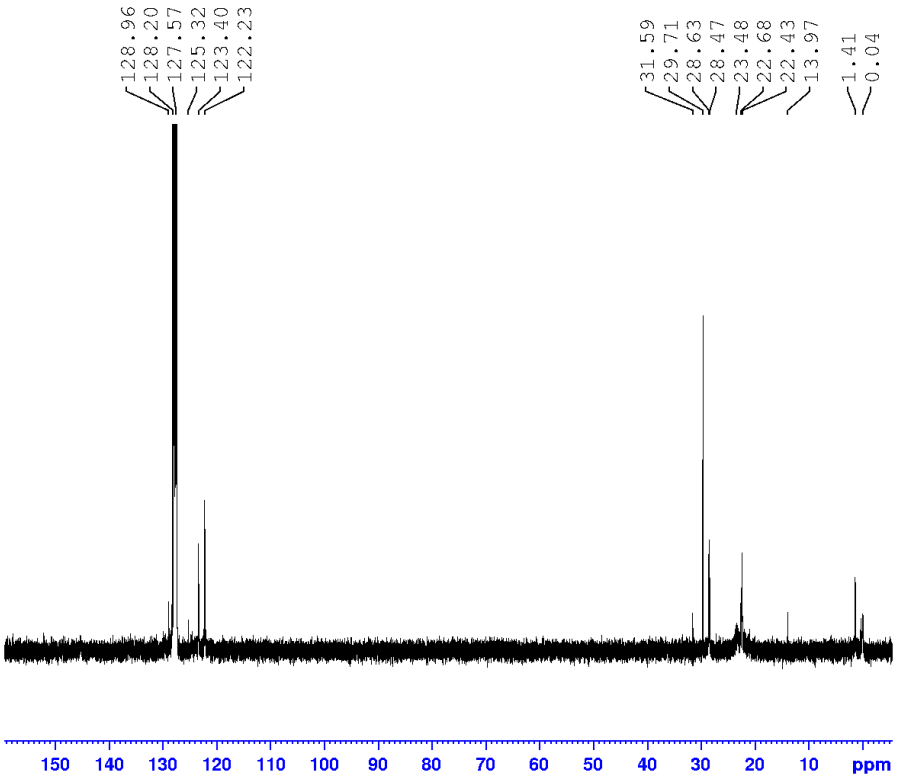

Figure S15. $^{13}C\{^{1}H\}$ NMR spectrum of **3b** in C_6D_6

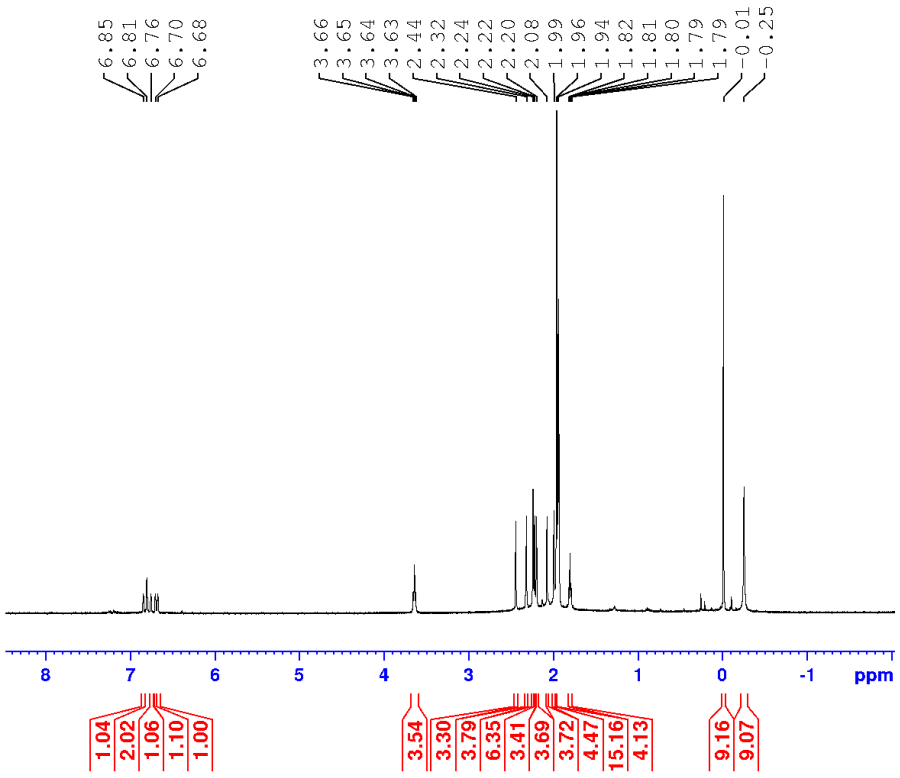

Figure S16. ^{1}H NMR spectrum of **4a** in CD_3CN

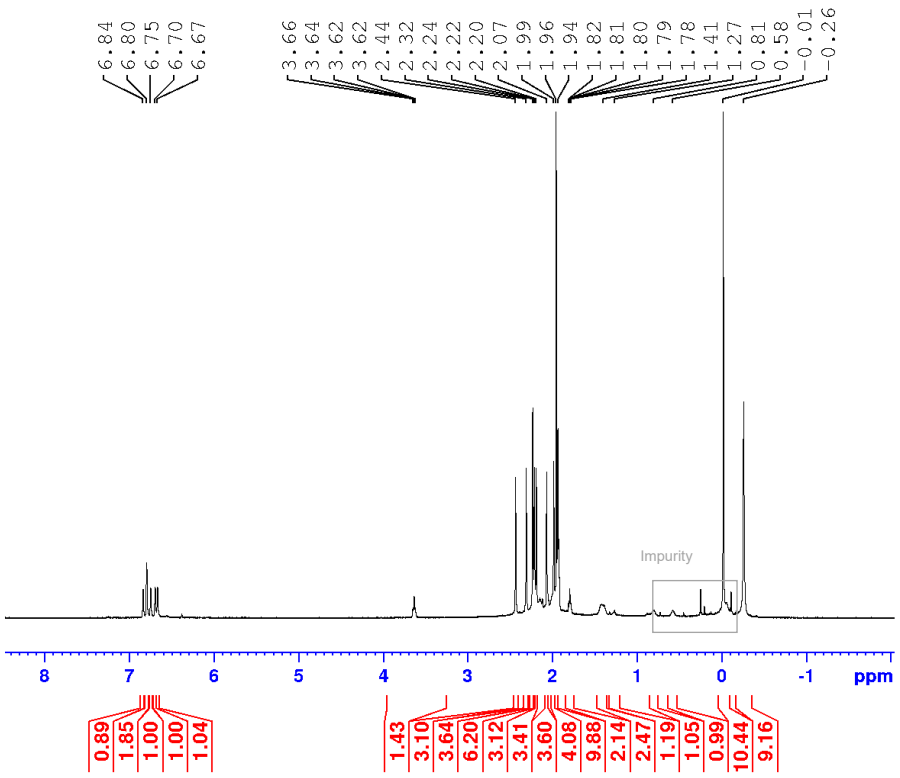

Figure S17. $^{1}H\{^{11}B\}$ NMR spectrum of **4a** in CD_3CN

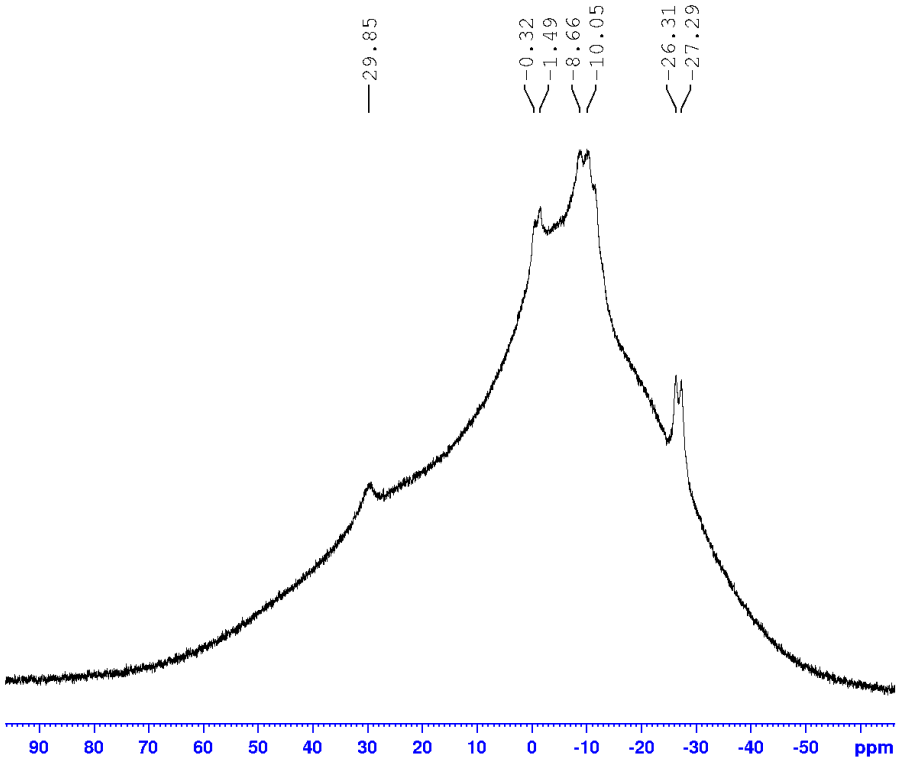

Figure S18. ^{11}B NMR spectrum of **4a** in CD_3CN

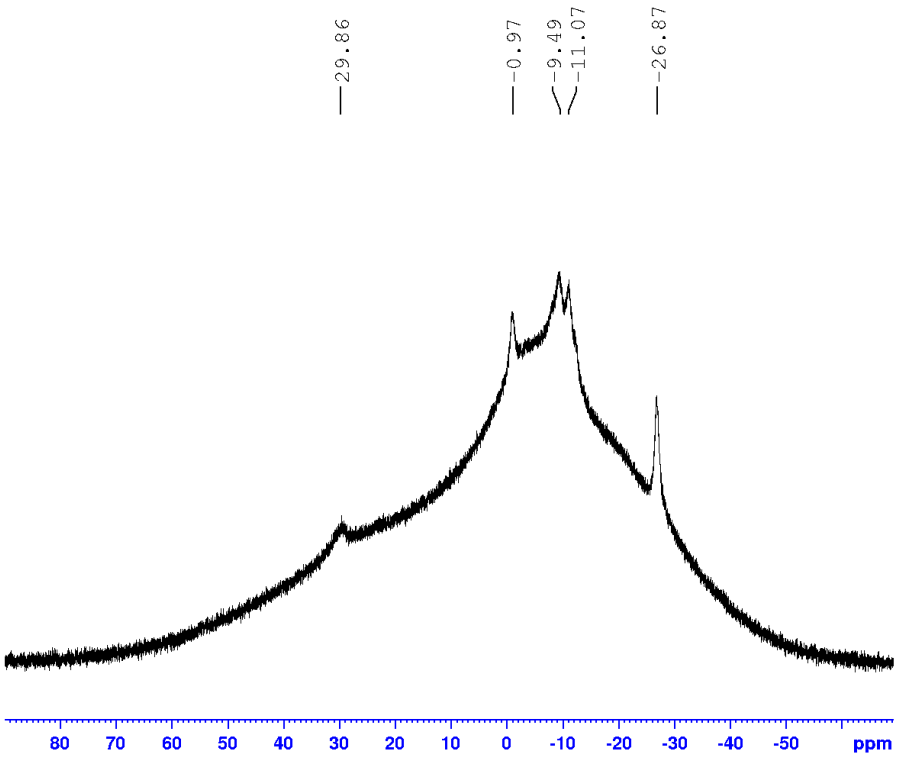

Figure S19. $^{11}B\{^{1}H\}$ NMR spectrum of **4a** in CD_3CN

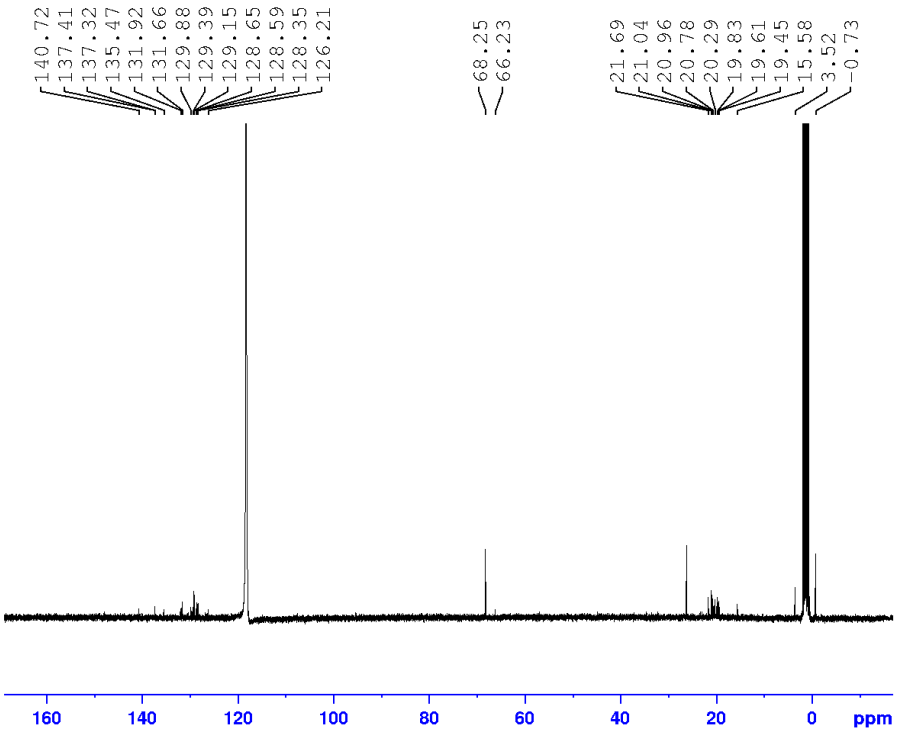

Figure S20. $^{13}C\{^{1}H\}$ NMR spectrum of **4a** in CD_3CN

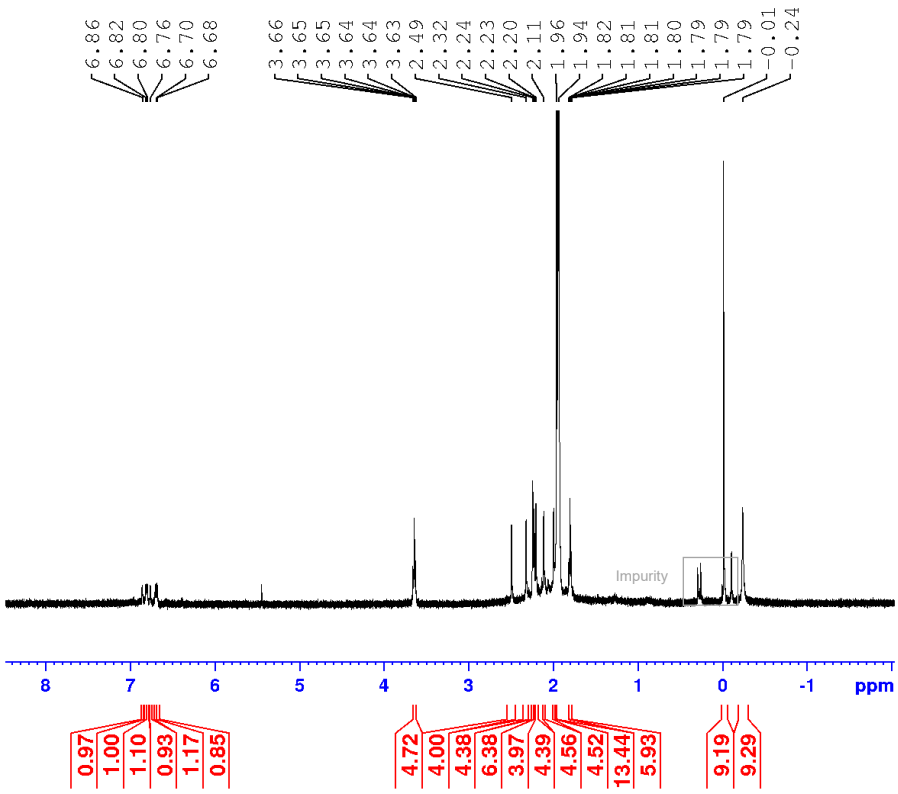

Figure S21. ^{1}H NMR spectrum of **4b** in CD_3CN

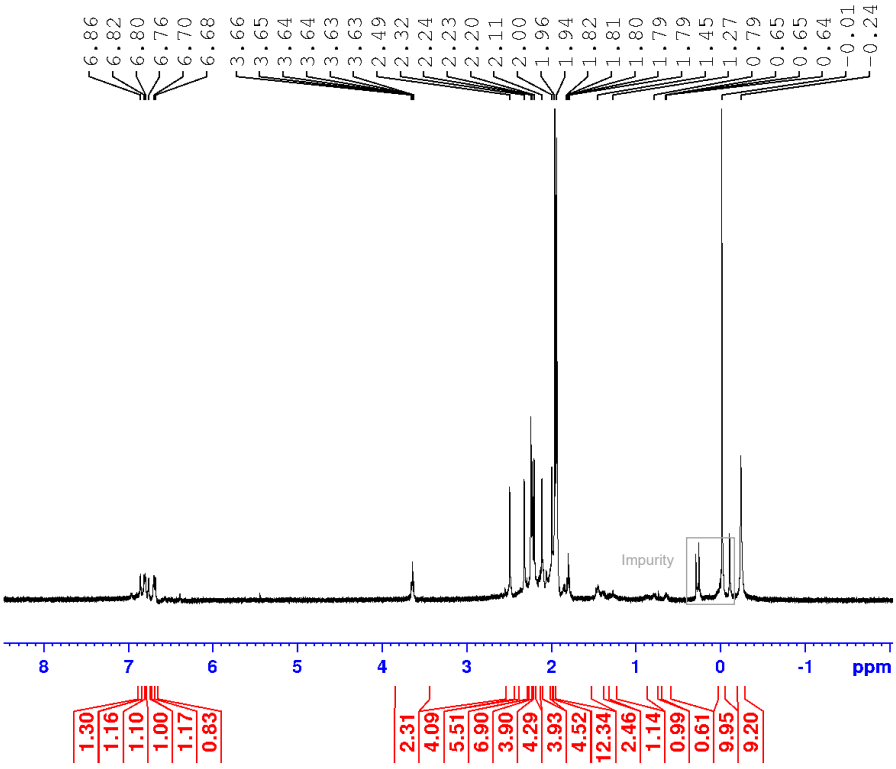

Figure S22. $^{1}H\{^{11}B\}$ NMR spectrum of **4b** in CD_3CN

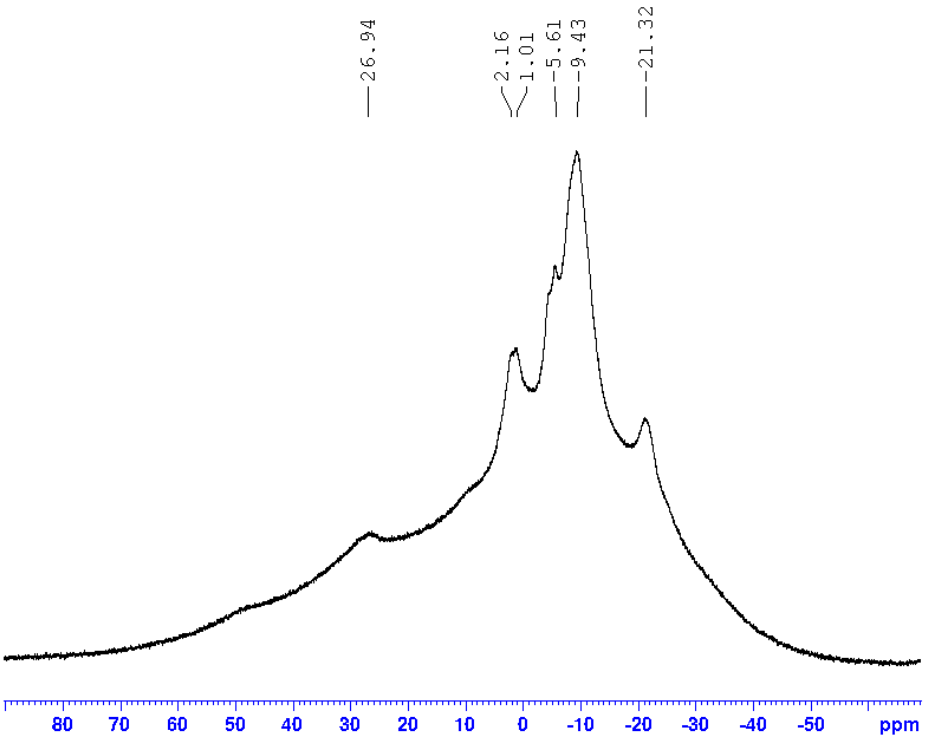

Figure S23. ^{11}B NMR spectrum of **4b** in CD_3CN

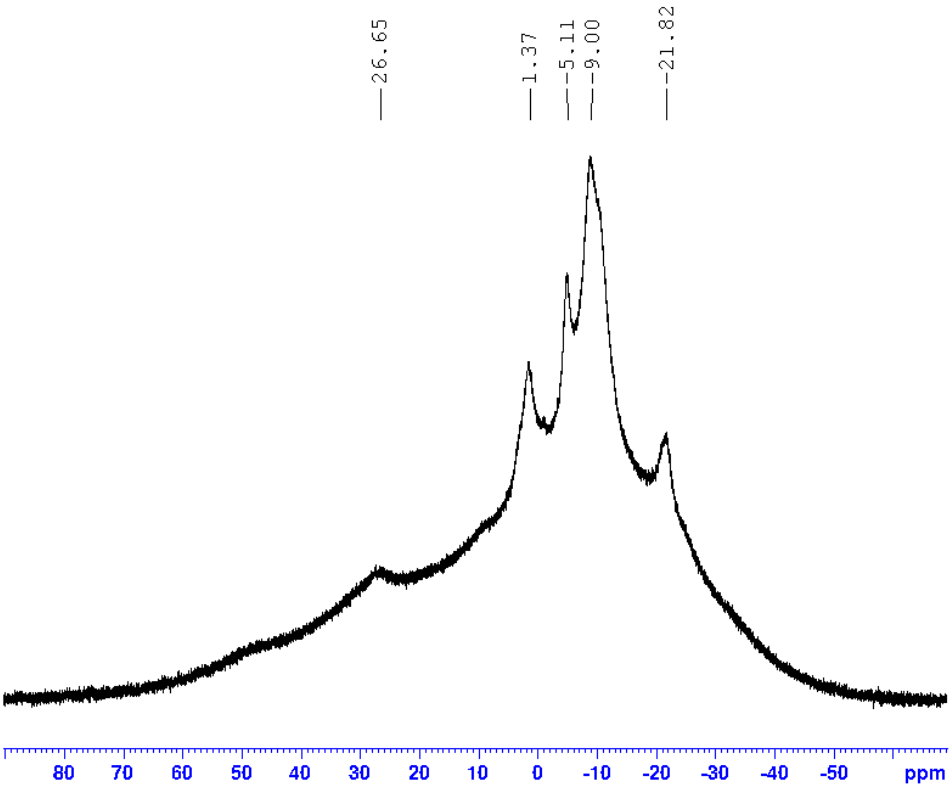

Figure S24. $^{11}B\{^1H\}$ NMR spectrum of **4b** in CD_3CN

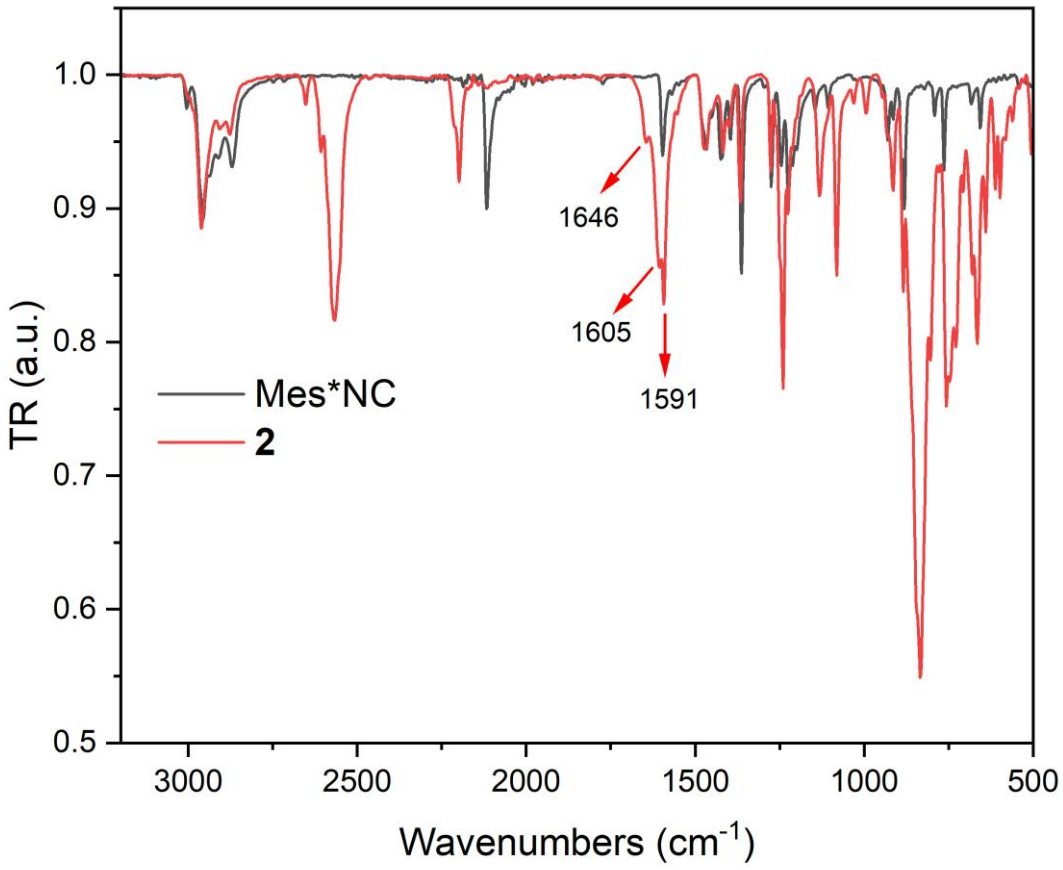

Figure S25. IR spectrum of **2**.

Crystal Data

The crystal data of **2**, **3a**, **3b**, **4a** and **4b** were collected on a Rigaku XtaLAB Synergy-R diffractometer with a HPA area detector and multi-layer mirror monochromated $Cu_{K\alpha}$ radiation. Data reduction, scaling and absorption corrections were performed using SAINT (Bruker, V8.38A, 2013). The structure was solved with the XT structure solution program using the Intrinsic Phasing solution method[2] and by using Olex as the graphical interface. The model was refined with the ShelXL program[3] using Least Squares minimization. All non-hydrogen atoms were refined anisotropically. Hydrogen atoms were included in structure factor calculations. All hydrogen atoms were assigned to idealized geometric positions. The structure was solved using intrinsic phasing method[2], refined with the ShelXL program[4] and expanded using Fourier techniques.

Crystallographic data has been deposited with the Cambridge Crystallographic Data as supplementary publication nos. CCDC 2504504-2504508. These data can be obtained free of charge from The Cambridge Crystallographic Data Centre via Data https://www.ccdc.cam.ac.uk

Table S1: Crystal data and structure refinement.

Identification code	**2**	**3a**
Empirical formula	$C_{27}H_{57}B_{11}N_2Si_2$	$C_{38}H_{61}B_{11}N_4Si_2$
Formula weight	584.83	748.99
Temperature/K	100(2)	100(2)
Crystal system	triclinic	monoclinic
Space group	P-1	$P2_1/c$
a/Å	11.3302(3)	13.7127(2)
b/Å	11.9721(2)	25.3195(3)
c/Å	28.1532(6)	13.17870(10)
α/°	91.080(2)	90
β/°	91.634(2)	103.6140(10)
γ/°	101.979(2)	90
Volume/Å^3	3733.00(14)	4447.07(9)
Z	4	4
ρ_{calc}g/cm^3	1.041	1.119
μ/mm^{-1}	0.987	0.948
F(000)	1264.0	1600.0
Crystal size/mm^3	0.25 × 0.18 × 0.16	0.22 × 0.1 × 0.04
Radiation	$Cu_{K\alpha}$ (λ = 1.54184)	$Cu_{K\alpha}$ (λ = 1.54184)
2Θ range for data collection/°	6.284 to 143.118	6.982 to 147.642
Index ranges	-13 ≤ h ≤ 13, -14 ≤ k ≤ 14, -33 ≤ l ≤ 33	-16 ≤ h ≤ 16, -31 ≤ k ≤ 30, -16 ≤ l ≤ 14
Reflections collected	20426	44752
Independent reflections	20426 [R_{int} = 0.0658, R_{sigma} = 0.0277]	8850 [R_{int} = 0.0480, R_{sigma} = 0.0316]
Data/restraints/parameters	20426/0/788	8850/0/511
Goodness-of-fit on F^2	1.029	1.049
Final R indexes [I>=2σ (I)]	R_1 = 0.0406, wR_2 = 0.1035	R_1 = 0.0396, wR_2 = 0.1054
Final R indexes [all data]	R_1 = 0.0454, wR_2 = 0.1066	R_1 = 0.0457, wR_2 = 0.1089
Largest diff. peak/hole / e Å^{-3}	0.27/-0.31	0.38/-0.34

Table S2: Crystal data and structure refinement.

Identification code	**3b**	**4a**	**4b**
Empirical formula	$C_{47}H_{79}B_{11}N_4Si_2$	$C_{48.55}H_{79.37}B_{11}N_{6.73}O_{1.27}Si_2Ca$	$C_{48}H_{78}B_{11}N_7OMgSi_2$
Formula weight	875.23	992.85	968.57
Temperature/K	100(2)	100(2)	100(2)
Crystal system	monoclinic	triclinic	triclinic
Space group	$P2_1/c$	P-1	P-1
a/Å	16.1104(2)	11.2865(2)	10.6536(2)
b/Å	12.03240(10)	13.2089(2)	12.6438(3)
c/Å	27.5466(3)	22.3633(2)	22.2211(6)
α/°	90	91.6240(10)	89.441(2)
β/°	94.3110(10)	90.6350(10)	78.944(2)
γ/°	90	108.4440(10)	71.061(2)
Volume/Å^3	5324.71(10)	3160.74(8)	2774.20(12)
Z	4	2	2
ρ_{calc}g/cm^3	1.092	1.043	1.160
μ/mm^{-1}	0.854	1.497	1.001
F(000)	1888.0	1062.0	1036.0
Crystal size/mm^3	0.12 × 0.1 × 0.08	0.1 × 0.08 × 0.07	0.17 × 0.08 × 0.05
Radiation	$Cu_{K\alpha}$ (λ = 1.54184)	$Cu_{K\alpha}$ (λ = 1.54184)	$Cu_{K\alpha}$ (λ = 1.54184)
2Θ range for data collection/°	5.502 to 150.254	7.058 to 146.934	7.404 to 146.416
Index ranges	-19 ≤ h ≤ 19, -14 ≤ k ≤ 10, -33 ≤ l ≤ 33	-13 ≤ h ≤ 13, -15 ≤ k ≤ 16, -27 ≤ l ≤ 27	-11 ≤ h ≤ 13, -15 ≤ k ≤ 15, -27 ≤ l ≤ 27
Reflections collected	51877	130343	53247
Independent reflections	10588 [R_{int} = 0.0340, R_{sigma} = 0.0303]	12082 [R_{int} = 0.0582, R_{sigma} = 0.0312]	10617 [R_{int} = 0.0304, R_{sigma} = 0.0255]
Data/restraints/parameters	10588/0/595	12082/195/695	10617/0/649
Goodness-of-fit on F^2	1.015	1.038	1.056
Final R indexes [I>=2σ (I)]	R_1 = 0.0435, wR_2 = 0.1029	R_1 = 0.0530, wR_2 = 0.1432	R_1 = 0.0409, wR_2 = 0.1102
Final R indexes [all data]	R_1 = 0.0572, wR_2 = 0.1095	R_1 = 0.0709, wR_2 = 0.1529	R_1 = 0.0488, wR_2 = 0.1148
Largest diff. peak/hole / e Å^{-3}	0.26/-0.32	0.57/-0.42	0.32/-0.31

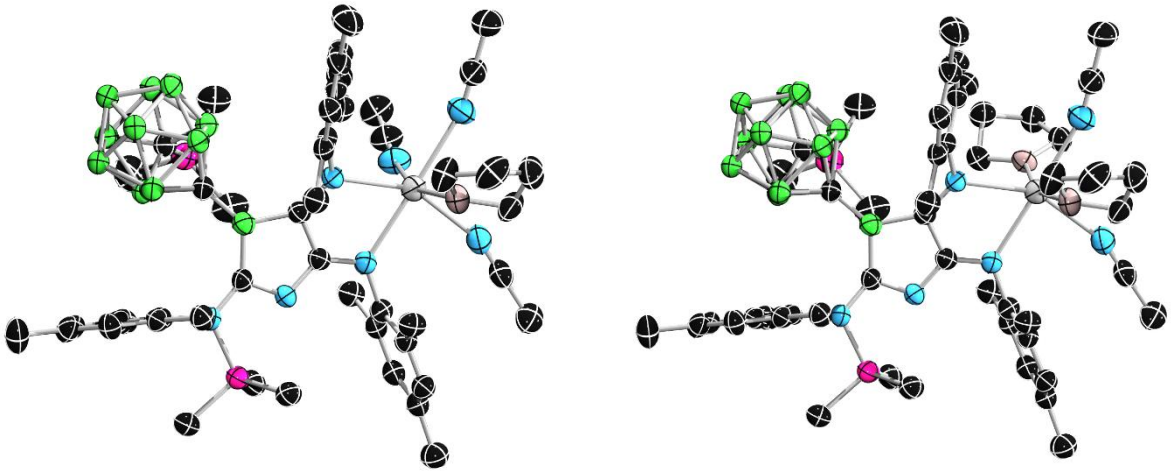

Figure S26. Solid-state structure of **4a** showing a disordered solvent site modelled as two alternative coordination modes: isocyanide-bound species (occupancy 0.73, left) and THF-bound species (occupancy 0.27, right). Hydrogen atoms omitted for clarity. Ellipsoids are shown at 50% probability.

Cyclic Voltammetry

A standard three-electrode cell configuration was employed using a platinum disk working electrode, a platinum wire counter electrode, and a silver wire, separated by a Vycor tip, serving as the reference electrode. Formal redox potentials are referenced to the ferrocene/ferrocenium ($[Cp_2Fe]^{+/0}$) redox couple by using decamethylferrocene ($[Cp^*_2Fe]$, $E1/2$ = −0.427 V in THF) as an internal standard. Tetra(*n*-butyl)ammonium hexafluorophosphate ($[nBu_4N][PF_6]$ was employed as the supporting electrolyte. Compensation for resistive losses (*iR* drop) was employed for all measurements.

Cyclic voltammetry (CV) analysis of compound **3a** was performed in THF with $[nBu_4N][PF_6]$ as the supporting electrolyte (Figure S27). The distinct redox events were observed: a cathodic wave at –1.94 V and an anodic wave at 0.44 V versus Fc/Fc^+. Both processes appear chemically irreversible under the experimental conditions, suggesting substantial structural reorganization or follow-up reactivity upon electron transfer.

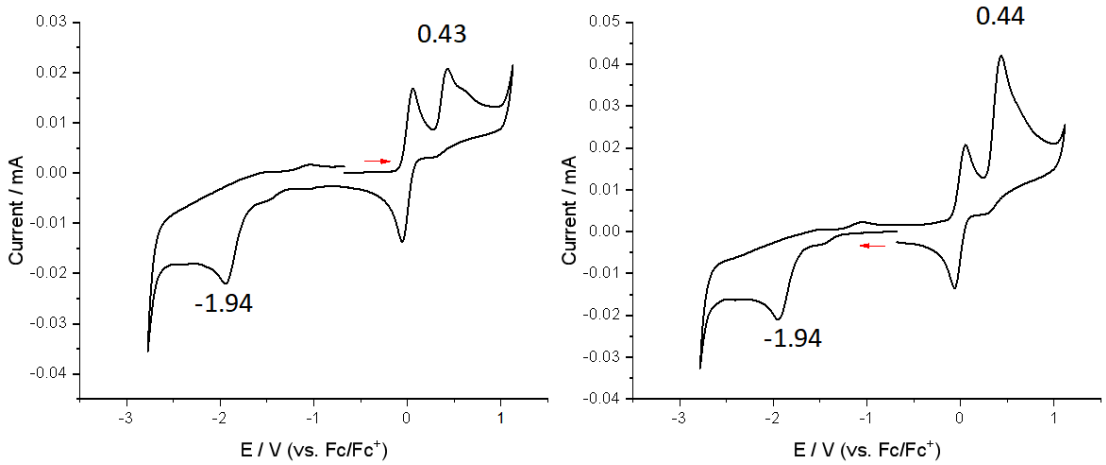

Figure S27. Cyclic voltammograms of **3a** in THF/0.1 M $[nBu_4N][PF_6]$ recorded with a scan rate of 250 mV s^{-1} in the anodic (left) and cathodic (right) direction.

UV-Vis Spectra

The UV-Vis absorption spectra of **4a** and **4b** were recorded in toluene under argon, exhibiting an absorption band (centered at 515 (**4a**) and 524 (**4b**)) in the visible region.

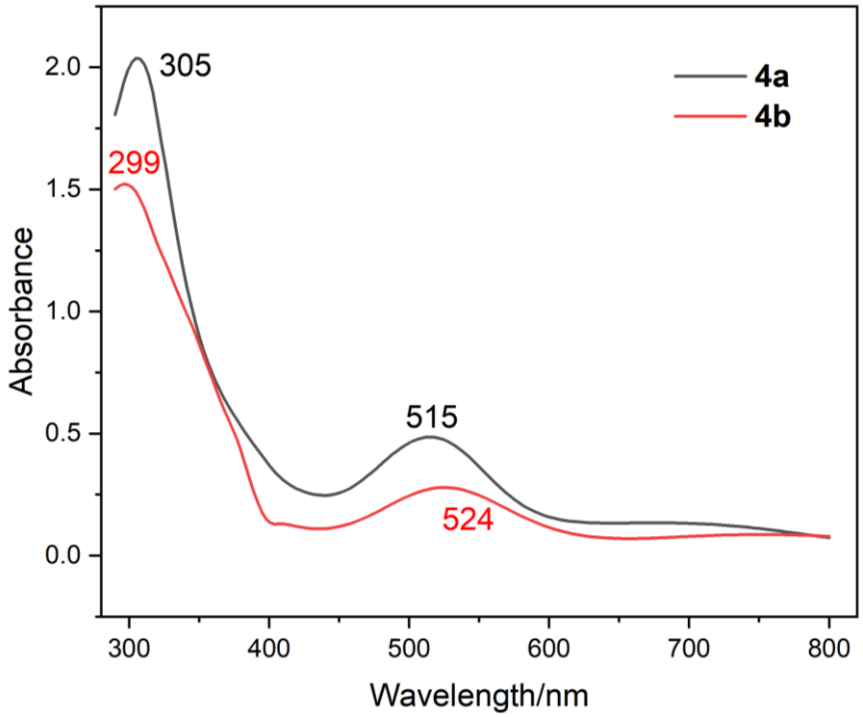

Figure S28. UV−Vis absorption spectra of **4a** and **4b** recorded in toluene (5.9×10^{-4} M) at room temperature.

Computational Details

All the calculations were carried out at the Gaussian 16 program.[5] All structures were optimized at the B3LYP hybrid functional with the D3 dispersion correction.[6] The def2TZVP basis set was used for Ca and the def2SVP basis set for the other atoms.[7] At the same level of theory, we performed the nucleus-independent chemical shift (NICS) calculations[8] and canonical molecular orbital (CMO) analysis. Frequency calculations were performed to (1) confirm that all the stationary points had no imaginary frequency and that each transition state structure had only one imaginary frequency, and (2) to obtain the relative Gibbs free energies at 298K. Intrinsic reaction coordinate (IRC) calculations were carried out to confirm that each transition state links the relevant local minima appropriately.

Based on the optimized structures, single-point energy calculations were re-calculated using the def2TZVP basis set was used for all the atoms.[7] The SMD solvation model[9] with n-pentane as the solvent was also employed in the single-point energy calculations.

We have also employed the M06-2-X functional[10] to perform geometry optimization for those structures involved in the first couple of steps presented in Figure 4 for comparison. The results now are included in the Computational Details section in the SI (Figure S29). both methods lead to similar qualitative and quantitative conclusions, highlighting the robustness of our mechanistic analysis.

a) Computed at the B3LYP-D3/Def2tzvp//B3LYP-D3/Def2svp level (reported in the main text)

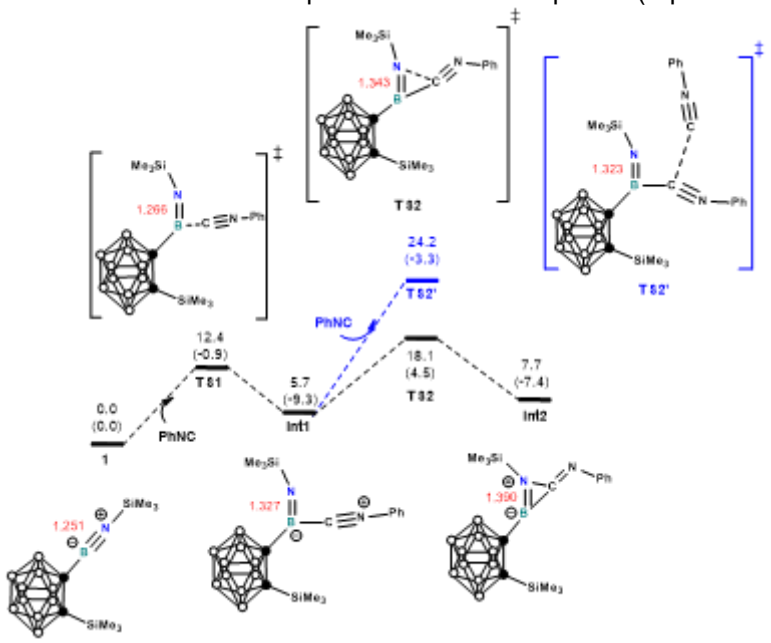

b) Computed at the M06-2X/Def2tzvp//M06-2X/Def2svp level (for comparison purpose)

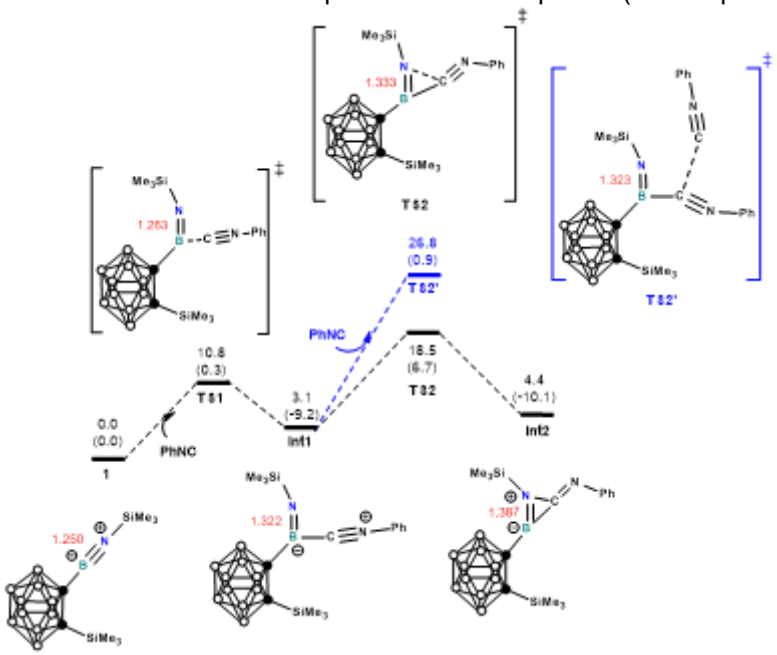

Figure S29. Comparison of DFT results obtained from B3LYP-D3 (a) and M06-2-X (b) calculations. Relative Gibbs free energies and electronic energies (in parentheses) are given in kcal/mol.

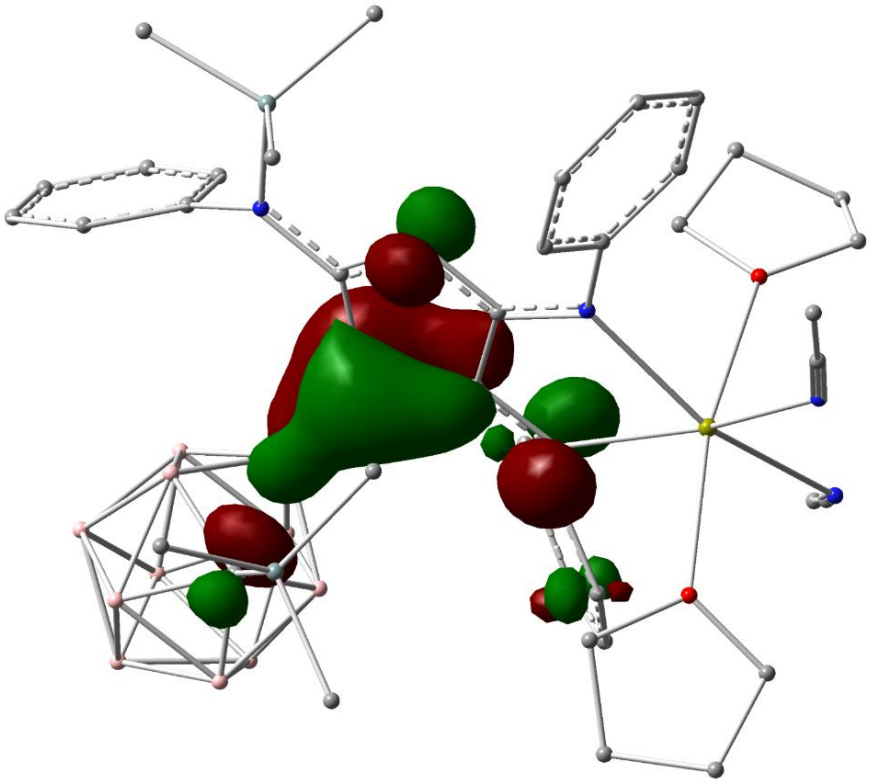

Figure S30. Plot of the highest occupied molecular orbital (HOMO) of **4a'.** Hydrogen atoms have been removed for clarity.

References

[1] Wang, J, Jia, P, Sun, W. Wei, Y, Lin, Z.; Ye, Q. *Inorg. Chem.* **2022**, *61*, 8879–8886.

[2] Sheldrick, G. *Acta Cryst.* **2015**, *A71*, 3–8.

[3] Sheldrick, G. *Acta Cryst.* **2008**, *A64*, 112–122.

[4] Frisch, M. J.; Trucks, G. W.; Schlegel, H. B.; Scuseria, G. E.; Robb, M. A.; Cheeseman, J. R.;Scalmani, G.; Barone, V.; Mennucci, B.; Petersson, G. A.; Nakatsuji, H.; Caricato, M.; Li, X.;Hratchian, H. P.; Izmaylov, A. F.; Bloino, J.; Zheng, G.; Sonnenberg, J. L.; Hada, M.; Ehara, M.;Toyota, K.; Fukuda, R.; Hasegawa, J.; Ishida, M.; Nakajima, T.; Honda, Y.; Kitao, O.; Nakai, H.;Vreven, T.; Montgomery, Jr., J. A.; Peralta, J. E.; Ogliaro, F.; Bearpark, M.; Heyd, J. J.; Brothers, E.;Kudin, K. N.; Staroverov, V. N.; Kobayashi, R.; Normand, J.; Raghavachari, K.; Rendell, A.; Burant,J. C.; Iyengar, S. S.; Tomasi, J.; Cossi, M.; Rega, N.; Millam, J. M.; Klene, M.; Knox, J. E.; Cross, J.B.; Bakken, V.; Adamo, C.; Jaramillo, J.; Gomperts, R.; Stratmann, R. E.; Yazyev, O.; Austin, A. J.; Cammi, R.; Pomelli, C.; Ochterski, J. W.; Martin, R. L.; Morokuma, .; Zakrzewski, V. G.; Voth, G.A.; Salvador, P.; Dannenberg, J. J.; Dapprich, S.; Daniels, A. D.; Farkas, Ö.; Foresman, J. B.; Ortiz, J. V.; Cioslowski, J.; Fox, D. J. Gaussian 09, Revision D.01; Gaussian, Inc.: Wallingford, CT, 2009.

[5] Gaussian 16, Revision C.01, M. J. Frisch, G. W. Trucks, H. B. Schlegel, G. E. Scuseria, M. A. Robb, J. R. Cheeseman, G. Scalmani, V. Barone, G. A. Petersson, H. Nakatsuji, X. Li, M. Caricato, A. V. Marenich, J. Bloino, B. G. Janesko, R. Gomperts, B. Mennucci, H. P. Hratchian, J. V. Ortiz, A. F. Izmaylov, J. L. Sonnenberg, D. Williams-Young, F. Ding, F. Lipparini, F. Egidi, J. Goings, B. Peng, A. Petrone, T. Henderson, D. Ranasinghe, V. G. Zakrzewski, J. Gao, N. Rega, G. Zheng, W. Liang, M. Hada, M. Ehara, K. Toyota, R. Fukuda, J. Hasegawa, M. Ishida, T. Nakajima, Y. Honda, O. Kitao, H. Nakai, T. Vreven, K. Throssell, J. A. Montgomery, Jr., J. E. Peralta, F. Ogliaro, M. J. Bearpark, J. J. Heyd, E. N. Brothers, K. N. Kudin, V. N. Staroverov, T. A. Keith, R. Kobayashi, J. Normand, K. Raghavachari, A. P. Rendell, J. C. Burant, S. S. Iyengar, J. Tomasi, M. Cossi, J. M. Millam, M. Klene, C. Adamo, R. Cammi, J. W. Ochterski, R. L. Martin, K. Morokuma, O. Farkas, J. B. Foresman, and D. J. Fox, Gaussian, Inc., Wallingford CT, 2016.

[6] (a) Grimme, S.; Antony, A.; Ehrlich, S.; Krieg, H. A consistent and accurate *ab initio* parametrization of density functional dispersion correction (DFT-D) for the 94 elements H-Pu. *J. Chem. Phys.*, **2010**, *132*, 154104. (b) Grimme, S.; Ehrlich, S.; Goerigk, L. Effect of the damping function in dispersion corrected density functional theory. *J. Comput. Chem.*, **2011**, *32*, 1456–1465.

[7] Weigend, F.; Ahlrichs, R. Balanced basis sets of split valence, triple zeta valence and quadruple zeta valence quality for H to Rn: Design and assessment of accuracy. *Physical Chemistry Chemical Physics* **2005**, *7*, 3297–3305. Weigend, F. Accurate Coulomb-fitting basis sets for H to Rn. *Physical chemistry chemical physics* **2006**, *8*, 1057–1065. Schäfer, A.; Horn, H.; Ahlrichs, R. Fully optimized contracted Gaussian basis sets for atoms Li to Kr. *J. Chem. Phys.* **1992**, *97*, 2571–2577. Schäfer, A.; Huber, C.; Ahlrichs, R. Fully optimized contracted Gaussian basis sets of triple zeta valence quality for atoms Li to Kr. *J. Chem. Phys.* **1994**, *100*, 5829–5835.

[8] Chen, Z.; Wannere, C. S.; Corminboeuf, C.; Puchta, R.; Schleyer, P. v. R. Nucleus independent chemical shifts (NICS) as an aromaticity criterion. *Chem. Rev*. **2005**, *105*, 3842–3888.

[9] Marenich, A. V.; Cramer, C. J.; Truhlar, D. G. Generalized born solvation model SM12. *J. Chem. Theory Comput.* **2013**, *9*, 609–620.

[10] Zhao, Y.; Truhlar, D. G. The M06suite of density functionals for main group thermochemistry, thermochemical kinetics, noncovalent interactions, excited states, and transition elements: two new functionals and systematic testing of four M06-class functionals and 12 other functionals. *Theor. Chem. Acc*. **2008**, *120*, 215–241.